Available online at www.sciencedirect.com
ScienceDirect
International Journal of Thermal Sciences 48 (2009) 699–707
International Journal of Thermal Sciences
www.elsevier.com/locate/ijts

Wall coupling effect in channel forced convection with streamwise periodic boundary heat flux variation

Antonio Barletta [a,*], Eugenia Rossi di Schio [a], Gianni Comini [b], Paola D'Agaro [b]

[a] *Alma Mater Studiorum – Università di Bologna, Dipartimento di Ingegneria Energetica, Nucleare e de Controllo Ambientale (DIENCA), Laboratorio di Montecuccolino, via dei Colli 16, 40136 Bologna, Italy*

[b] *Università degli Studi di Udine, Dipartimento di Energetica e Macchine, Via delle Scienze 208, 33100 Udine, Italy*

Received 4 April 2008; received in revised form 30 May 2008; accepted 13 June 2008

Available online 7 July 2008

Abstract

The present paper deals with the laminar forced convection in a parallel-plane channel, and is aimed to investigate the effect of conducting walls. On the external boundaries of the duct walls a thermal boundary condition is prescribed, such that the wall heat flux longitudinally varies with sinusoidal law. The local energy balance equation is written separately for the fluid and the solid regions, with reference to the fully developed regime, and then solved both analytically and numerically. Moreover, the local and average Nusselt numbers in a longitudinal period are evaluated. The average Nusselt number, if regarded as a function of the dimensionless pulsation, displays an interesting feature. In fact, for all the considered cases, it has a minimum, so that there exists a value of the dimensionless pulsation such that the heat exchange between the fluid and the solid wall is considerably inhibited.

Keywords: Laminar flow; Forced convection; Conjugate problem; Finite element method; Analytical solution

1. Introduction

The present paper aims to extend a previous analysis, performed under the hypothesis of a temperature field longitudinally varying with sinusoidal law [1]. The study referred to the case of a longitudinally periodic boundary condition given by the temperature distribution on the external boundary of the solid walls.

There are many applications consisting of periodic repetitions of a particular geometric or heating unit. Examples are, for instance, chips located on a circuit board, internally finned ducts, heat exchangers with regularly spaced turbulence promoters, cooling system of nuclear reactors. As is well known, although in the case of prescribed temperature boundary conditions the flow in these geometries is asymptotically isothermal, this does not happen in the case of prescribed wall heat flux. Some papers deal with periodic thermal profiles induced by periodic geometries, with reference both to forced [2,3] and mixed convection [4].

In the literature, boundary conditions implying a periodic change of the heat flux have deserved great attention, with reference to forced convection [5–8]. Pearlstein and Dempsey [5] report the temperature field distribution and the bulk temperature in the thermal inlet region, for various values of the Peclet number. An axially varying wall heat flux is assumed. In [6] and [7], the thermally developed forced convection is investigated analytically, by considering and by neglecting axial heat conduction effects. Reference is made to a cylindrical duct with circular cross section and to a wall heat flux which axially varies with sinusoidal law. It is shown that in the thermally developed region the temperature distribution is given by the sum of a linear and a periodic function of the axial coordinate. Moreover, in [8], the effect of a transverse magnetic field is taken into account. In none of the above mentioned papers conducting walls are considered.

The aim of the present paper is to investigate the conjugate heat transfer in a parallel plane channel, by considering the ef-

* Corresponding author.
E-mail addresses: antonio.barletta@unibo.it (A. Barletta), eugenia.rossidischio@unibo.it (E. Rossi di Schio), gianni.comini@uniud.it (G. Comini), dagaro.paola@uniud.it (P. D'Agaro).

1290-0729/$ – see front matter
doi:10.1016/j.ijthermalsci.2008.06.003

Nomenclature

B	dimensionless pulsation defined in Eq. (7)
C_1, C_2, C_3	constants defined in Eq. (22)
$\hat{C}_1$, $\hat{C}_2$, $\hat{C}_3$	constants defined in Eq. (39)
${}_1F_1$	confluent hypergeometric function
f	complex dimensionless function
G	complex dimensionless parameter
H	complex dimensionless parameter
i	imaginary unit
k	thermal conductivity
L	length of the computational domain
Nu	Nusselt number, defined by Eq. (24)
$\overline{Nu}$	average value of the Nusselt number in a longitudinal period, defined by Eq. (31)
n	positive integer
Pe	Peclet number, defined in Eq. (7)
q	thermal heat flux prescribed on the external boundary of the channel walls
q_0	mean value of the thermal heat flux prescribed on the external boundary of the channel walls
T	temperature
T_0	inlet temperature
U	longitudinal component of the fluid velocity
U_0	mean value of the fluid velocity
y	spatial coordinate
y_0	internal channel half-height
y_1	external channel half-height
z	longitudinal coordinate
z_i	longitudinal position of the inlet section

Greek symbols

α	thermal diffusivity
β	pulsation
γ	dimensionless parameter, defined in Eq. (7)
ζ	longitudinal dimensionless coordinate, defined in Eq. (7)
η	spatial dimensionless coordinate, defined in Eq. (7)
θ	dimensionless temperature, defined in Eq. (7)
$\hat{\theta}$	dimensionless temperature, defined in Eq. (36)
λ	dimensionless parameter, defined in Eq. (1)
ξ	complex dimensionless variable
σ	dimensionless half-width of the channel, defined in Eq. (7)
φ_i	dimensionless heat flux at the interface, defined by Eq. (35)
φ_σ	dimensionless heat flux on the external boundary, defined by Eq. (9)
ϕ	dimensionless complex heat flux at the interface, defined by Eq. (29)
ψ	dimensionless complex temperature
$\hat{\psi}$	dimensionless complex temperature, defined in Eq. (36)

Operators

∇	dimensionless gradient

Subscripts

b	bulk quantity
f	fluid
s	solid

fect of forced convection in the fluid and conduction in the channel walls. On the external boundary of the channel walls a thermal boundary condition is prescribed, such that the heat flux is a periodic function of the longitudinal coordinate having mean value q_0. Axial heat conduction and viscous dissipation in the fluid will be neglected, and reference will be made to the fully developed region. The energy local balance equation will be solved both analytically, by employing the confluent hypergeometric functions theory, and numerically, by employing a finite element procedure described, in detail, in [9,10]. The numerical procedure, designed for problems characterized by complex geometries and boundary conditions, had been repeatedly validated by comparison with numerical solutions and experimental results concerning uncoupled problems (see, for example, Refs. [11,12]). Here the validation process is completed for situations in which conduction and convection effects are simultaneously present.

2. Mathematical model

Let us consider an infinitely long parallel-plane channel. The two channel walls, having distance $2y_0$, are $y_1 - y_0$ thick. Due to the symmetry on the plane $y = 0$, the analysis will be devoted to the region $0 \leqslant y \leqslant y_1$. The longitudinal section of the parallel-plane channel, together with the boundary conditions, is reported in Fig. 1.

Let us consider a Newtonian fluid with constant thermophysical properties, in a fully developed forced convection regime, such that viscous dissipation and longitudinal heat conduction in the fluid can be neglected. Let us assume that on the external boundaries of the channel walls, a heat flux distribution is prescribed, namely:

$$k_s \left.\frac{\partial T}{\partial y}\right|_{y=y_1} = q_0\left[1 + \lambda \sin(\beta z)\right]. \tag{1}$$

In the fully developed region the local energy balance equation for the fluid is given by

$$U\frac{\partial T}{\partial z} = \alpha_f \frac{\partial^2 T}{\partial y^2}, \tag{2}$$

while for the solid ($y_0 < y < y_1$) one has

$$\frac{\partial^2 T}{\partial y^2} + \frac{\partial^2 T}{\partial z^2} = 0, \tag{3}$$

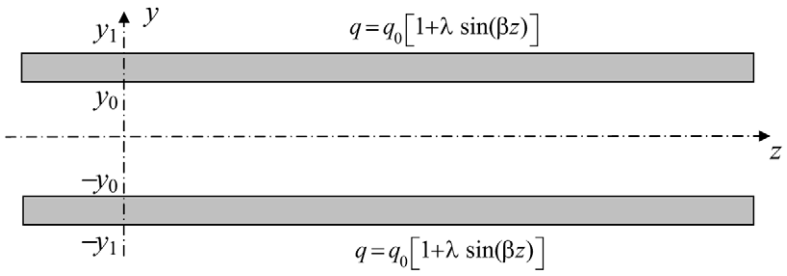

Fig. 1. Channel section.

where the subscript f refers to the fluid and U represents the velocity distribution in the fluid, given by the well-known Poiseuille profile

$$U(y)=\frac{3U_0}{2}\left[1-\left(\frac{y}{y_0}\right)^2\right]. \tag{4}$$

The equations have to be solved together with the boundary condition, taking into account the symmetry at $y=0$

$$\left.\frac{\partial T}{\partial y}\right|_{y=0}=0, \tag{5}$$

and with the matching conditions at $y=y_0$, namely

$$T_f(y_0,z)=T_s(y_0,z),\qquad k_f\left.\frac{\partial T}{\partial y}\right|_{f,y=y_0}=k_s\left.\frac{\partial T}{\partial y}\right|_{s,y=y_0}. \tag{6}$$

Let us introduce the following dimensionless quantities:

$$\eta=\frac{y}{y_0},\quad \zeta=\frac{z}{y_0},\quad \sigma=\frac{y_1}{y_0},\quad \theta=k_f\frac{T-T_0}{q_0y_0},$$
$$\gamma=\frac{k_s}{k_f},\qquad Pe=\frac{U_0y_0}{\alpha_f},\qquad B=Pe\,\beta y_0. \tag{7}$$

It is then possible to write the dimensionless local balance equations for the fluid and the solid regions respectively as:

$$\frac{3}{2}\left(1-\eta^2\right)\frac{\partial\theta}{\partial\zeta}=\frac{1}{Pe}\frac{\partial^2\theta}{\partial\eta^2},\quad 0<\eta<1,$$
$$\frac{\partial^2\theta}{\partial\eta^2}+\frac{\partial^2\theta}{\partial\zeta^2}=0,\qquad 1<\eta<\sigma, \tag{8}$$

with the boundary condition

$$\gamma\left.\frac{\partial\theta}{\partial\eta}\right|_{s,\eta=\sigma}=1+\lambda\sin\left(\frac{B\zeta}{Pe}\right)=\varphi_\sigma(\zeta), \tag{9}$$

with the symmetry condition at $\eta=0$

$$\left.\frac{\partial\theta}{\partial\eta}\right|_{\eta=0}=0, \tag{10}$$

and with the matching conditions at $\eta=1$

$$\theta_f(1,\zeta)=\theta_s(1,\zeta),\qquad \left.\frac{\partial\theta}{\partial\eta}\right|_{f,\eta=1}=\gamma\left.\frac{\partial\theta}{\partial\eta}\right|_{s,\eta=1}. \tag{11}$$

For longitudinal positions sufficiently distant from the inlet section of the duct, placed at $z=z_i$, one can assume that the solution of Eq. (8) has the form:

$$\theta(\eta,\zeta)=\frac{A\zeta}{Pe}+\theta_0(\eta)+\theta_1(\eta)\sin\left(\frac{B\zeta}{Pe}\right)+\theta_2(\eta)\cos\left(\frac{B\zeta}{Pe}\right), \tag{12}$$

where the constant A and the functions $\theta_0(\eta)$, $\theta_1(\eta)$ and $\theta_2(\eta)$ can be determined by substituting Eq. (12) into Eqs. (8)–(11). One obtains three boundary value problems:

$$\begin{cases}0<\eta<1\to \mathrm{d}^2\theta_0(\eta)/\mathrm{d}\eta^2=(3/2)A(1-\eta^2),\\ 1<\eta<\sigma\to \mathrm{d}^2\theta_0(\eta)/\mathrm{d}\eta^2=0,\\ \mathrm{d}\theta_0/\mathrm{d}\eta|_{\eta=0}=0,\\ \theta_{0,f}(1)=\theta_{0,s}(1),\\ \mathrm{d}\theta_0/\mathrm{d}\eta|_{f,\eta=1}=\gamma\,\mathrm{d}\theta_0/\mathrm{d}\eta|_{s,\eta=1},\\ \gamma\,\mathrm{d}\theta_0/\mathrm{d}\eta|_{\eta=\sigma}=1;\end{cases} \tag{13}$$

$$\begin{cases}0<\eta<1\to \mathrm{d}^2\theta_1(\eta)/\mathrm{d}\eta^2=-(3/2)(1-\eta^2)B\theta_2(\eta),\\ 1<\eta<s\to \mathrm{d}^2\theta_1(\eta)/\mathrm{d}\eta^2=(B^2/Pe^2)\theta_1(\eta),\\ \mathrm{d}\theta_1/\mathrm{d}\eta|_{\eta=0}=0,\\ \theta_{1,f}(1)=\theta_{1,s}(1),\\ \mathrm{d}\theta_1/\mathrm{d}\eta|_{f,\eta=1}=\gamma\,\mathrm{d}\theta_1/\mathrm{d}\eta|_{s,\eta=1},\\ \gamma\mathrm{d}\theta_1/\mathrm{d}\eta|_{\eta=\sigma}=\lambda;\end{cases} \tag{14}$$

$$\begin{cases}0<\eta<1\to \mathrm{d}^2\theta_2(\eta)/\mathrm{d}\eta^2=(3/2)(1-\eta^2)B\theta_1(\eta),\\ 1<\eta<s\to \mathrm{d}^2\theta_2(\eta)/\mathrm{d}\eta^2=(B^2/Pe^2)\theta_2(\eta),\\ \mathrm{d}\theta_2/\mathrm{d}\eta|_{\eta=0}=0,\\ \theta_{2,f}(1)=\theta_{2,s}(1),\\ \mathrm{d}\theta_2/\mathrm{d}\eta|_{f,\eta=1}=\gamma\,\mathrm{d}\theta_2/\mathrm{d}\eta|_{s,\eta=1},\\ \gamma\mathrm{d}\theta_2/\mathrm{d}\eta|_{\eta=\sigma}=0.\end{cases} \tag{15}$$

The boundary value problems described by Eqs. (14) and (15) can be collapsed into a unique boundary value problem for the complex function $\psi(\eta)=\theta_1(\eta)+i\theta_2(\eta)$, which represents the *complex temperature*. One obtains

$$\begin{cases}0<\eta<1\to \mathrm{d}^2\psi(\eta)/\mathrm{d}\eta^2-(3/2)i\,B(1-\eta^2)\psi(\eta)=0,\\ 1<\eta<\sigma\to \mathrm{d}^2\psi(\eta)/\mathrm{d}\eta^2-(B^2/Pe^2)\psi(\eta)=0,\\ \mathrm{d}\psi/\mathrm{d}\eta|_{\eta=0}=0,\\ \psi_f(1)=\psi_s(1),\\ \mathrm{d}\psi/\mathrm{d}\eta|_{f,\eta=1}=\gamma\,\mathrm{d}\psi/\mathrm{d}\eta|_{s,\eta=1},\\ \gamma\mathrm{d}\psi/\mathrm{d}\eta|_{\eta=\sigma}=\lambda.\end{cases} \tag{16}$$

The solution of the boundary value problem (13) yields

$$0<\eta<1\rightarrow\theta_0(\eta)=\frac{3}{4}A\eta^2-\frac{1}{8}A\eta^4+C_0,$$
$$1<\eta<\sigma\rightarrow\theta_0(\eta)=\frac{\eta}{\gamma}+D_0. \tag{17}$$

By employing the matching conditions, one obtains

$$A=1,\quad D_0=C_0+\frac{5}{8}-\frac{1}{\gamma}. \tag{18}$$

Since the temperature field, for the considered boundary condition, is defined up to an arbitrary additive constant, one can assume $C_0=0$. One has

$$0<\eta<1\rightarrow\theta_0(\eta)=\frac{3}{4}\eta^2-\frac{1}{8}\eta^4,$$
$$1<\eta<\sigma\rightarrow\theta_0(\eta)=\frac{\eta}{\gamma}+\frac{5}{8}-\frac{1}{\gamma}. \tag{19}$$

The solution of the boundary value problem (16) allows one to determine the temperature distribution, for the solid and the fluid regions separately. For the fluid region $0<\eta<1$, if one redefines the unknown function and the independent variable in Eq. (16) as

$$\xi=-\frac{H}{2}\eta^2,\qquad f=e^{-\frac{H}{4}\eta^2}\psi(\eta),$$

where $H=(i-1)\sqrt{3B}$, one can easily verify that function $f(\xi)$ fulfills the confluent hypergeometric equation [13]. On account of the symmetry condition in $\eta=0$, one obtains

$$\psi(\eta)=C_1e^{H\eta^2/4}\,{}_1F_1\left(\frac{2+H}{8};\frac{1}{2};-\frac{H}{2}\eta^2\right), \tag{20}$$

where C_1 is an integration constant to be determined through the matching conditions and ${}_1F_1$ is the confluent hypergeometric function.

For the solid region, $1<\eta<\sigma$, one has

$$\psi(\eta)=C_2e^{\eta B/Pe}+C_3e^{-\eta B/Pe}, \tag{21}$$

where the integrations constants have to be obtained prescribing the boundary condition in $\eta=\sigma$ and the matching conditions. Finally, one obtains

$$C_1=\frac{e^{(1-\sigma)B/Pe}Pe\lambda/(B\gamma)+C_3[e^{-B/Pe}+e^{(1-2\sigma)B/Pe}]}{{}_1F_1(\frac{2+H}{8};\frac{1}{2};-\frac{H}{2})e^{H/4}},$$
$$C_2=C_3e^{-2\sigma B/Pe}+\frac{\lambda}{\gamma}\frac{Pe}{B}e^{-\sigma B/Pe},$$
$$C_3=-\frac{e^{B(2+\sigma)/Pe}Pe(GPe+B\gamma)\lambda}{B\gamma[e^{2B\sigma/Pe}(GPe-B\gamma)+e^{2B/Pe}(GPe+B\gamma)]}, \tag{22}$$

where the parameter

$$G=\frac{H(2+H)\,{}_1F_1(\frac{10+H}{8};\frac{3}{2};-\frac{H}{2})}{4\,{}_1F_1(\frac{2+H}{8};\frac{1}{2};-\frac{H}{2})}-\frac{H}{2} \tag{23}$$

has been introduced. By employing the dimensionless quantities, one can write the Nusselt number as

$$Nu=4y_0\frac{\partial T}{\partial y}\bigg|_{f,y=y_0}\big[T(y_0,z)-T_b(z)\big]^{-1}$$
$$=4\frac{\partial\theta}{\partial\eta}\bigg|_{f,\eta=1}\big[\theta(1,\zeta)-\theta_b(\zeta)\big]^{-1}, \tag{24}$$

where $4y_0$ is the hydraulic diameter and θ_b is the dimensionless bulk temperature, namely

$$\theta_b(\zeta)=\frac{3}{2}\int_0^1\theta(\eta,\zeta)\big(1-\eta^2\big)\,\mathrm{d}\eta. \tag{25}$$

By employing Eq. (12), the local Nusselt number can be rewritten as

$$Nu(\zeta)=4\bigg[\frac{\mathrm{d}\theta_1}{\mathrm{d}\eta}\bigg|_{f,\eta=1}\sin\left(\frac{B\zeta}{Pe}\right)+\frac{\mathrm{d}\theta_2}{\mathrm{d}\eta}\bigg|_{f,\eta=1}\cos\left(\frac{B\zeta}{Pe}\right)+\frac{\mathrm{d}\theta_0}{\mathrm{d}\eta}\bigg|_{f,\eta=1}\bigg]$$
$$\times\left\{\big[\theta_0(1)-\theta_{0b}\big]+\big[\theta_1(1)-\theta_{1b}\big]\sin\left(\frac{B\zeta}{Pe}\right)+\big[\theta_2(1)-\theta_{2b}\big]\cos\left(\frac{B\zeta}{Pe}\right)\right\}^{-1}, \tag{26}$$

where θ_{1b} and θ_{2b} are the real and imaginary part respectively of

$$\psi_b=\frac{3}{2}\int_0^1\psi(\eta)\big(1-\eta^2\big)\,\mathrm{d}\eta. \tag{27}$$

If one integrates with respect to η the first of Eqs. (16), one obtains

$$\psi_b=-\frac{i}{B}\frac{\mathrm{d}\psi}{\mathrm{d}\eta}\bigg|_{f,\eta=1}=-\frac{i}{B}\phi, \tag{28}$$

where $\phi=\chi_1+i\chi_2$ is the complex heat flux at the interface, defined as

$$\phi=\gamma\frac{\mathrm{d}\psi}{\mathrm{d}\eta}\bigg|_{s,\eta=1}. \tag{29}$$

Thus, it is possible to rewrite Eq. (26) as follows:

$$Nu(\zeta)=4\left[1+\chi_1\sin\left(\frac{B\zeta}{Pe}\right)+\chi_2\cos\left(\frac{B\zeta}{Pe}\right)\right]$$
$$\times\left\{\frac{17}{35}+\left[\theta_1(1)-\frac{\chi_2}{B}\right]\sin\left(\frac{B\zeta}{Pe}\right)+\left[\theta_2(1)+\frac{\chi_1}{B}\right]\cos\left(\frac{B\zeta}{Pe}\right)\right\}^{-1}. \tag{30}$$

Finally, one can evaluate the average value of the Nusselt number in a longitudinal period:

$$\overline{Nu}=\frac{B}{2\pi Pe}\int_0^{2\pi\,Pe/B}Nu(\zeta)\,\mathrm{d}\zeta. \tag{31}$$

3. Numerical solution

The use of the finite element method allows one to solve more complicated forms of the problem under exam. One can deal with more realistic geometries of the channel including, for instance, cases with internal longitudinal or transverse fins. In general, for complicated geometries of the channel and in

the presence of fins, analytical solutions for the velocity and temperature fields are not available. The comparison between the analytical solution available in the elementary case examined in the present paper and the numerical solution obtained through a finite-element method appears as very important for a validation of the procedure.

In stationary regime, with reference to a fluid having constant thermophysical properties, by neglecting internal heat sources and viscous dissipation effects, the energy equation has the following dimensionless form:

$$(\mathbf{u}\cdot\nabla)\theta = \frac{1}{Pe}\nabla^2\theta. \tag{32}$$

In a conjugate heat transfer problem, Eq. (32) is solved for the whole domain, by assuming, for each region, the corresponding thermophysical properties and by prescribing $\mathbf{u} = 0$ in the solid region [11]. The continuity of temperature at the solid–fluid interface is then ensured through the energy equation, and there is no need to prescribe it explicitly.

For the problem considered here, the computational domain is a portion of parallel plane channel, in the thermally fully developed region, having length $L = 2\pi/\beta$, i.e. length equal to an oscillation period of the sinusoidal heat flux prescribed on the external boundary of the wall (Eq. (9)). However, the symmetry condition (Eq. (10)) allows one to study half of the domain.

The mean value q_0 of the heat flux distribution (Eq. (1)) induces a constant increase of the temperature between the inlet and outlet sections of the periodic module. As a consequence, the longitudinal conduction fluxes entering and leaving the solid region have the same absolute value and do not contribute to the energy balance. Therefore, the temperature increase in the fluid region can be directly related to the imposed flux q_0 by the expression

$$T\left(y, \frac{2\pi}{\beta}\right) - T(y,0) = q_0\frac{\alpha_f}{k_f}. \tag{33}$$

The same temperature increase is induced also in the solid region since fluid and solid temperatures cannot diverge. Thus Eq. (33), written in the dimensionless form

$$\theta\left(\eta, \frac{2\pi\, Pe}{B}\right) = \theta(\eta,0) + \frac{2\pi}{B} \tag{34}$$

can be utilized as a boundary condition for the inlet and outlet sections of both the fluid and solid regions. It can be easily verified, in fact, that Eq. (34) is perfectly consistent with the assumed form (12) of the analytical solution.

At this point, to complete the formulation of boundary conditions, we only have to prescribe the temperature level by imposing the value of temperature in a single point of the domain.

After obtaining a temperature solution, the dimensionless heat flux at the solid–fluid interface is evaluated as

$$\varphi_i(\zeta) = \gamma\left.\frac{\partial\theta}{\partial\eta}\right|_{s,\eta=1}, \tag{35}$$

while the average Nusselt number is evaluated by Eq. (31).

With reference to the imposed temperature level and to the analytical expression of the velocity field (Eq. (4)), Eqs. (32) and (34) are solved by the finite element algorithm, described in detail in [9]. It must be pointed out that the spatial discretization, described in [9], is based on the Bubnov–Galerkin method, so that the numerical diffusivity, typical of the upwind schemes, is not introduced.

Simulations have been done for $Pe = 100$ and $\sigma = 1.2$, for different values of the dimensionless parameter B (in the range $B = 1 \div 100$), two values of the ratio γ ($\gamma = 0.5, 3$) and two values of the parameter λ ($\lambda = 0.5, 1$). The computational grids already used in [1] are employed once again here. They are defined on the computational domains having dimensionless height 1 and dimensionless axial lengths ranging from 200π (for $B = 1$) to π ($B = 100$). The grids are uniformly spaced in both the axial and the transverse direction and utilize a constant number of 16 nodes in the transverse direction. In the axial direction, a number of 501 equally spaced nodes has been applied in the range $B = 5 \div 100$ and it has been increased to 1501 and 3001 for the cases $B = 2$ and $B = 1$, respectively. The accuracy reached in this way has been extensively discussed in [1], demonstrating the achievement of a relative accuracy of the order of 0.1% for the oscillation amplitude of the interface temperatures.

4. The case $\lambda \to \infty$

Let us now discuss the limiting case of purely sinusoidal temperature distribution. In order to investigate this case, let us redefine the dimensionless temperature and complex temperature as

$$\hat\theta = \frac{\theta}{\lambda}, \quad \hat\psi = \frac{\psi}{\lambda}. \tag{36}$$

By substituting Eq. (36) into Eq. (12) and by taking the limit $\lambda \to \infty$, one obtains

$$\hat\theta(\eta,\zeta) = \hat\theta_1(\eta)\sin\left(\frac{B\zeta}{Pe}\right) + \hat\theta_2(\eta)\cos\left(\frac{B\zeta}{Pe}\right), \tag{37}$$

where $\hat\theta_1$ and $\hat\theta_2$ are respectively the real and imaginary parts of the complex function $\hat\psi(\eta)$. On account of Eqs. (20)–(22) and (36), the function $\hat\psi(\eta)$ is given by

$$0 < \eta < 1 \to \hat\psi(\eta) = \hat C_1 e^{H\eta^2/4}\,{}_1F_1\left(\frac{2+H}{8}; \frac{1}{2}; -\frac{H}{2}\eta^2\right),$$
$$1 < \eta < \sigma \to \hat\psi(\eta) = \hat C_2 e^{\eta B/Pe} + \hat C_3 e^{-\eta B/Pe}, \tag{38}$$

where the constants are

$$\hat C_1 = \frac{e^{(1-\sigma)B/Pe}Pe/(B\gamma) + \hat C_3[e^{-B/Pe} + e^{(1-2\sigma)B/Pe}]}{{}_1F_1(\frac{2+H}{8}; \frac{1}{2}; -\frac{H}{2})e^{H/4}},$$
$$\hat C_2 = \hat C_3 e^{-2\sigma B/Pe} + \frac{Pe}{B\gamma}e^{-\sigma B/Pe},$$
$$\hat C_3 = -\frac{e^{B(2+\sigma)/Pe}Pe(G\,Pe + B\gamma)}{B\gamma[e^{2B\sigma/Pe}(G\,Pe - B\gamma) + e^{2B/Pe}(G\,Pe + B\gamma)]}, \tag{39}$$

and the parameter G, defined by Eq. (23), has been employed.

A comparison between Eqs. (20)–(21) and (38) shows that, in the limiting case of a sinusoidal wall heat flux with a vanishing mean value, only the integration constants are differently defined.

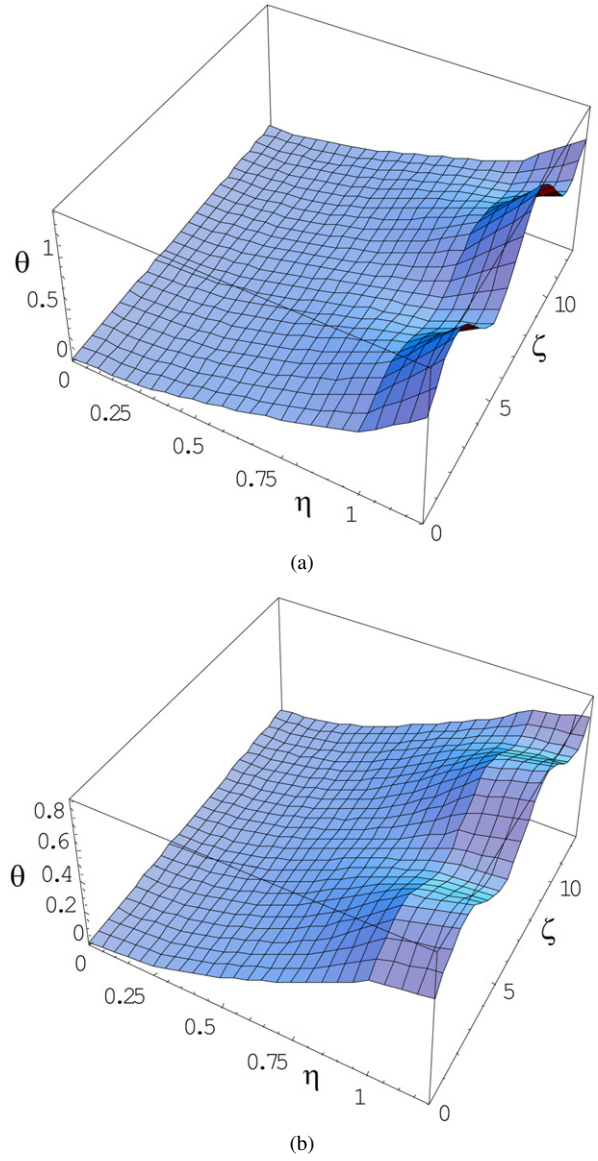

Fig. 2. Analytical solution: dimensionless temperature distribution $\theta(\eta, \zeta)$ for $\sigma = 1.2$, $Pe = 100$, $B = 100$, $\lambda = 0.5$ and $\gamma = 0.5$ (a), $\gamma = 3$ (b).

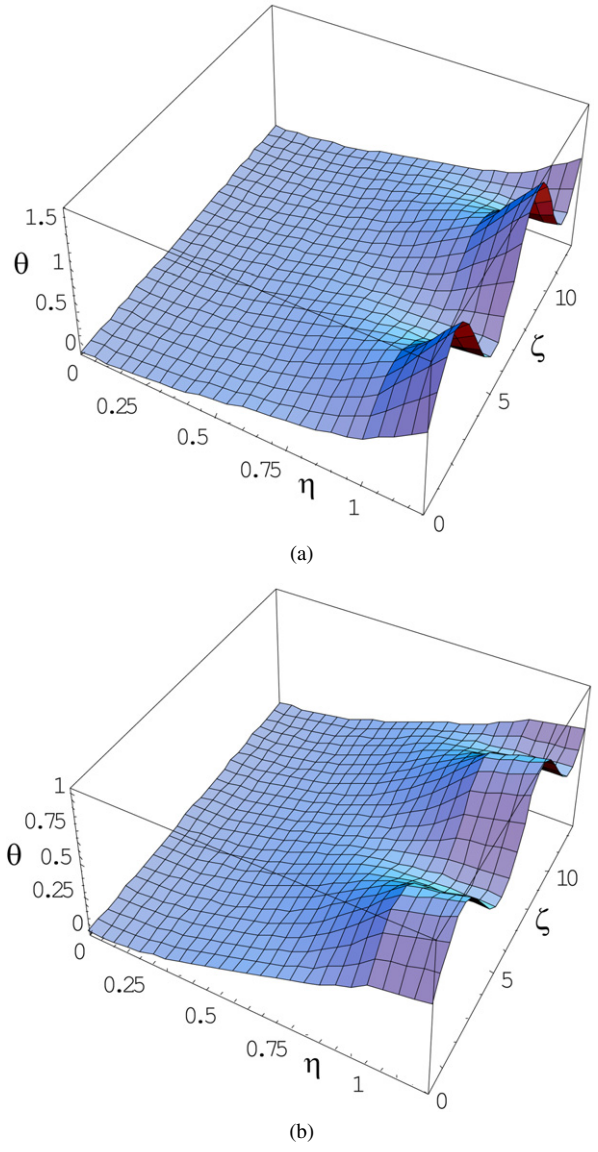

Fig. 3. Analytical solution: dimensionless temperature distribution $\theta(\eta, \zeta)$ for $\sigma = 1.2$, $Pe = 100$, $B = 100$, $\lambda = 1$ and $\gamma = 0.5$ (a), $\gamma = 3$ (b).

5. Discussion of the results

In Figs. 2 and 3 the temperature distribution is reported, for $\sigma = 1.2$ $B = 10$ and $Pe = 100$. Fig. 2 refers to $\lambda = 0.5$, while Fig. 3 refers to $\lambda = 1$. In both figures, the upper frame refers to $\gamma = 0.5$ while the lower one refers to $\gamma = 3$. The analysis of the two figures shows that, in the case of a wall less conducting than the fluid ($\gamma = 0.5$), both the longitudinal and the transverse components of the temperature gradient are higher in the solid wall than in the fluid.

In Figs. 4 and 5 the dimensionless temperature distribution is reported for $Pe = 100$, $B = 100$, $\sigma = 1.2$ and $\lambda = 1$. Fig. 4 refers to $\gamma = 0.5$, while Fig. 5 refers to $\gamma = 3$. The temperature fields have been obtained through the numerical solution.

In Figs. 6 and 7 the heat flux and temperature dimensionless distributions on the external boundary of the wall $\eta = \sigma$ and at the interface $\eta = 1$ are reported. Fig. 6 refers to the case $\gamma = 0.5$, while Fig. 7 refers to the case $\gamma = 3$. For $\gamma = 0.5$, the lag between the interface heat flux, with respect to the prescribed heat flux on the external boundary, is indiscernible, while the lags between temperature on the external boundary and temperature at the interface are 0.06π and 0.17π, respectively. For $\gamma = 3$, the interface heat flux displays a larger phase lag, namely 0.02π, while the lags of the temperature at the external boundary and at the interface are 0.11π and 0.16π, respectively.

In Table 1, values of the average Nusselt number, evaluated through Eq. (31), are reported versus the parameters B, γ and λ, together with the same values obtained numerically. The table refers to $Pe = 100$ and $\sigma = 1.2$ and shows that the average Nusselt number is not a monotonic function of B. In fact, for any given (γ, λ), first it decreases and then it increases with B. In the case $\lambda = 0$, one obtains for the average Nusselt number the value $140/17$. This is the well known asymptotic value for the fully developed forced convection in a parallel-plane chan-

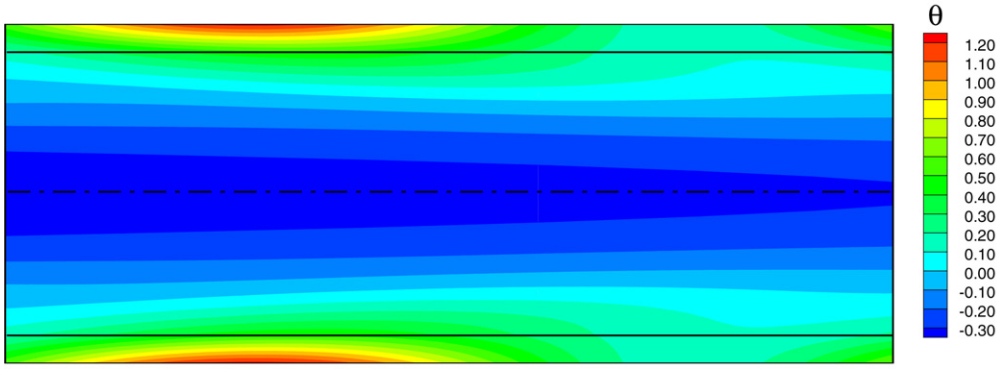

Fig. 4. Numerical solution: dimensionless temperature distribution $\theta(\eta, \zeta)$, for $\sigma = 1.2$, $Pe = 100$, $B = 100$, $\lambda = 1$ and $\gamma = 0.5$.

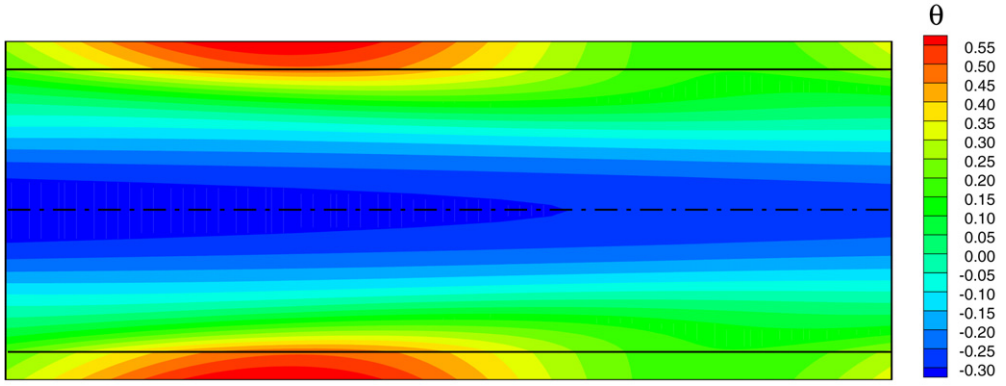

Fig. 5. Numerical solution: dimensionless temperature distribution $\theta(\eta, \zeta)$, for $\sigma = 1.2$, $Pe = 100$, $B = 100$, $\lambda = 1$ and $\gamma = 3$.

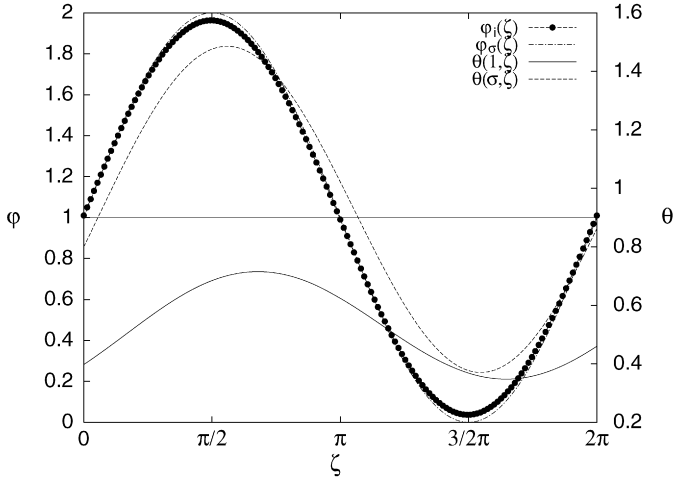

Fig. 6. Numerical solution: dimensionless heat flux φ and temperature θ distributions on the external boundary $\eta = \sigma$ and at the interface $\eta = 1$ for $\sigma = 1.2$, $\lambda = 1$, $\gamma = 0.5$, $Pe = 100$ and $B = 100$.

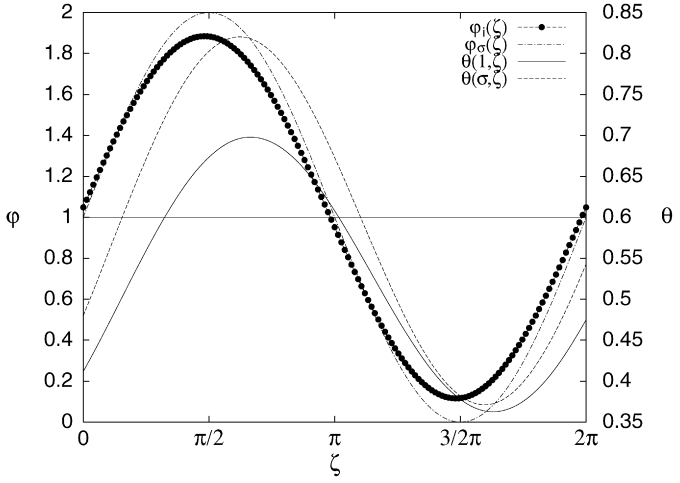

Fig. 7. Numerical solution: dimensionless heat flux φ and temperature θ distributions on the external boundary $\eta = \sigma$ and at the interface $\eta = 1$ for $\sigma = 1.2$, $\lambda = 1$, $\gamma = 3$, $Pe = 100$ and $B = 100$.

nel, with uniform wall heat flux boundary condition. Moreover, the table allows a comparison between the two solutions, thus revealing an excellent agreement. In fact, the relative error between the average Nusselt number values obtained analytically and numerically is always less than 0.06%.

In Figs. 8 and 9, the average Nusselt number in a longitudinal period is reported versus the dimensionless pulsation, for $Pe = 100$ and $\sigma = 1.2$. In Fig. 8, the influence of the conducting wall is pointed out. In fact, the two plots reported in this figure refer to different values of the ratio γ. On the other hand, Fig. 9 refers to two different values of λ and to $\gamma = 3$. Both figures show that, there exists a small value of the dimensionless pulsation such that the heat exchange between the fluid and the solid wall is considerably inhibited, especially when a boundary condition is prescribed such that the oscillation amplitude of the heat flux is equal to its mean value. Fig. 9 shows that if

Table 1
Values of the average Nusselt number, for $\sigma = 1.2$ and $Pe = 100$. Comparison between analytical solution and numerical solution (in italics)

B	$\overline{Nu}$			
	$\gamma = 0.5$		$\gamma = 3$	
	$\lambda = 0.5$	$\lambda = 1$	$\lambda = 0.5$	$\lambda = 1$
1	8.23356	8.07832	8.23356	8.07921
	8.238	*8.082*	*8.238*	*8.083*
2	8.22852	7.94249	8.22852	7.94429
	8.233	*7.946*	*8.233*	*7.948*
5	8.19874	7.64303	8.19879	7.64753
	8.203	*7.643*	*8.203*	*7.650*
10	8.13710	7.38607	8.13754	7.39256
	8.141	*7.387*	*8.141*	*7.397*
20	8.06627	7.23543	8.06856	7.25588
	8.070	*7.236*	*8.072*	*7.256*
50	8.03109	7.25762	8.04274	7.32394
	8.034	*7.256*	*8.046*	*7.322*
100	8.04454	7.39072	8.07516	7.53848
	8.047	*7.387*	*8.077*	*7.535*

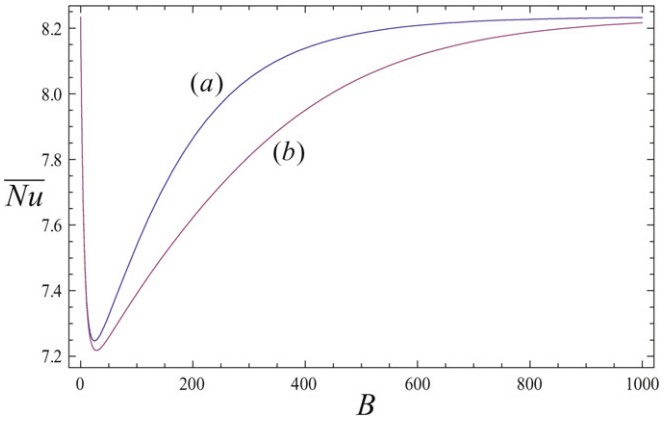

Fig. 8. Analytical solution: average Nusselt number versus the dimensionless pulsation, for $\sigma = 1.2$, $Pe = 100$, $\lambda = 1$ and $\gamma = 3$ (a), $\gamma = 0.5$ (b).

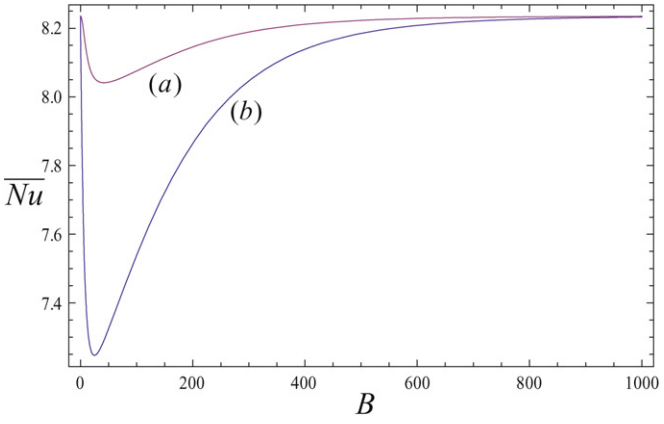

Fig. 9. Analytical solution: average Nusselt number versus the dimensionless pulsation, for $\sigma = 1.2$, $Pe = 100$, $\gamma = 3$ and $\lambda = 0.5$ (a), $\lambda = 1$ (b).

this oscillation amplitude is reduced, with respect to the mean value of the prescribed heat flux, the minimum reached by the average Nusselt number increases.

In Fig. 10, the case $\lambda \to \infty$ is investigated, i.e. the limiting case of a purely sinusoidal temperature distribution. In

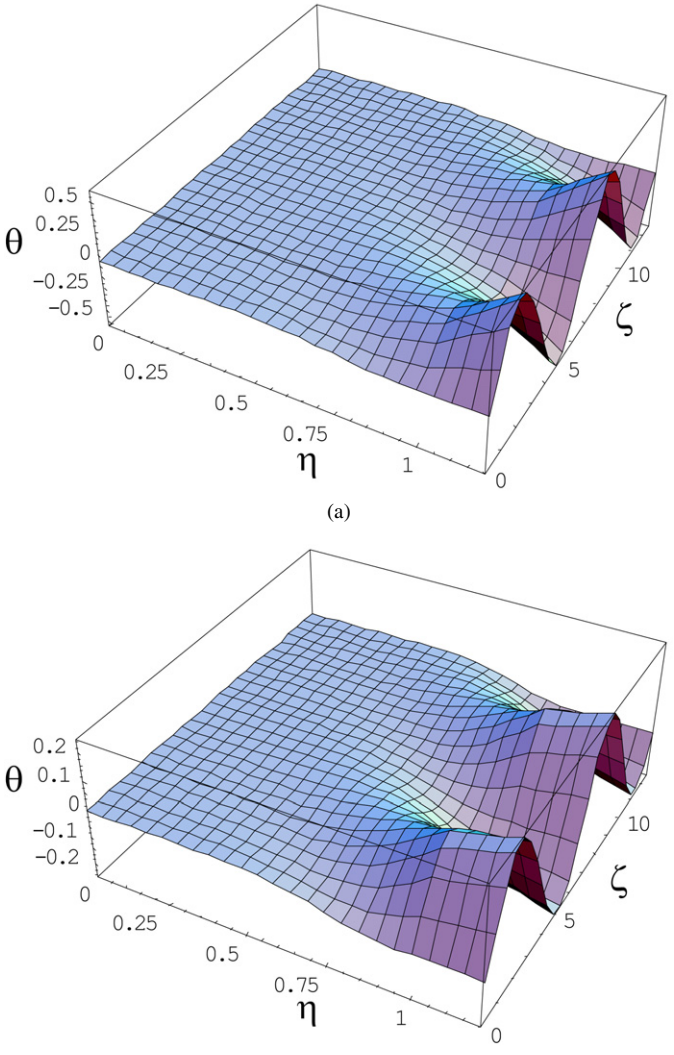

Fig. 10. Analytical solution: dimensionless temperature distribution $\hat{\theta}(\eta, \zeta)$ for $\sigma = 1.2$, $Pe = 100$, $B = 100$ and $\gamma = 0.5$ (a), $\gamma = 3$ (b) in the case $\lambda \to \infty$.

Fig. 10 the dimensionless temperature distribution $\hat{\theta}$ is reported for $Pe = 100$, $B = 100$ and $\sigma = 1.2$. The upper frame (a) refers to $\gamma = 0.5$, while the lower frame (b) refers to $\gamma = 3$. The figure shows that in this limiting case the longitudinal mean value of the temperature distribution is zero. For this choice of the parameters, the effect of the flux oscillations are very small in the fluid region.

6. Conclusions

In the present paper, the laminar forced convection in a plane-parallel channel is studied by taking into account the effect of the heat conduction in the channel walls having a finite thickness. On the external boundary of the channel walls a heat flux which varies longitudinally with sinusoidal law is prescribed. The local energy balance equation is solved both analytically and numerically, with reference to the fully developed region, where the temperature can be expressed as the sum of a linear and a periodic function of the longitudinal coordi-

nate. The analytical and numerical solutions reveal an excellent agreement.

The local Nusselt number is evaluated, as well as its mean value in a longitudinal period. The average Nusselt number, if regarded as a function of the dimensionless pulsation, displays an interesting feature. In fact, it displays a minimum: there exists a small value of the dimensionless pulsation such that the heat exchange between the fluid and the solid wall is considerably inhibited.

References

[1] A. Barletta, E. Rossi di Schio, G. Comini, P. D'Agaro, Conjugate forced convection heat transfer in a plane channel: Longitudinally periodic regime, International Journal of Thermal Sciences 47 (2008) 43–51.

[2] N.K. Ghaddar, G.E. Karniadakis, A.T. Patera, A conservative isoparametric spectral element method for forced convection; application to fully developed flow in periodic geometries, Numerical Heat Transfer 9 (1986) 277–300.

[3] Z.-X. Yuan, W.-Q. Tao, Q.-W. Wang, Numerical prediction for laminar forced convection heat transfer in a parallel-plate channels with streamwise periodic rod disturbances, International Journal for Numerical Methods in Fluids 28 (1998) 1371–1387.

[4] S.Y. Kim, H.J. Sung, J.M. Hyun, Mixed convection from multiple-layered boards with cross streamwise periodic boundary conditions, International Journal of Heat and Mass Transfer 35 (1992) 2941–2952.

[5] A.J. Pearlstein, B.P. Dempsey, Low Peclet number heat transfer in a laminar tube flow subjected to axially varying wall heat flux, ASME Journal of Heat Transfer 110 (1988) 796–798.

[6] A. Barletta, E. Zanchini, Laminar forced convection with sinusoidal wall heat flux distribution: Axially periodic regime, Heat and Mass Transfer 31 (1995) 41–48.

[7] A. Barletta, E. Rossi di Schio, Periodic forced convection with axial heat conduction in a circular duct, International Journal of Heat and Mass Transfer 43 (2000) 2949–2960.

[8] K. Zniber, A. Oubarra, J. Lahjomri, Analytical solution to the problem of heat transfer in an MHD flow inside a channel with prescribed sinusoidal wall heat flux, Energy Conversion and Management 46 (2005) 1147–1163.

[9] C. Nonino, G. Comini, An equal-order velocity-pressure algorithm for incompressible thermal flows. Part 1: Formulation, Numerical Heat Transfer B 32 (1997) 1–15.

[10] C. Nonino, G. Comini, Finite element analysis of convection problems in spatially periodic domains, Numerical Heat Transfer B 34 (1998) 361–378.

[11] G. Comini, C. Nonino, S. Savino, Modeling of coupled conduction and convection in moist air cooling, Numerical Heat Transfer A 51 (2007) 23–37.

[12] P. D'Agaro, G. Comini, Thermal performance evaluation of coolant passages with staggered arrays of pin fins, Heat and Mass Transfer 44 (2008) 815–825.

[13] M. Abramowitz, I.A. Stegun, Handbook of Mathematical Functions, Applied Mathematics Series, vol. 55, National Bureau of Standards, 1964 (Chapter 13).